Kinetics and Mechanism for Formation of Enols in Reaction of Hydroxide Radical with Propene

Chong-Wen Zhou,[†] Ze-Rong Li,[‡] and Xiang-Yuan Li*[,†]

College of Chemical Engineering and College of Chemistry, Sichuan University, Chengdu 610065, People's Republic of China

Received: September 27, 2008; Revised Manuscript Received: January 4, 2009

Recently, enols have been found to be the common intermediates in hydrocarbon combustion flames (Taatjes et al. *Science* **2005**, *308*, 1887), but the knowledge of kinetic properties for such species in combustion flames is rare. Therefore in this work, particular attention is paid to the formation of enols in combustion flames. Starting with HO and propene ($CH_3CH{=}CH_2$), the reaction mechanism involving eight product channels has been investigated systematically. It is revealed that the electrophilic addition of OH to the double bond of $CH_3CH{=}CH_2$ is unselective and the chemically activated adducts, $CH_3CHOH{=}CH_2$ and $CH_3CH{=}CH_2OH$, may undergo dissociation in competition with H-abstractions. The kinetics and product branching ratios of the HO and propene reaction have been evaluated in the temperature range of 200−3000 K by Variflex code, based on the weak collision master equation/microcanonical variational RRKM theory. Available experimental kinetic data can be quantitatively reproduced by this study, with a minor adjustment (1.0 kcal/mol) of the OH central addition barrier. From the theoretical calculations with multiple reflection correction included, the total rate constant is fitted to $k_t = 6.07 \times 10^{-5}T^{-2.54} \exp(108/T)$ cm^3·molecule^{-1}·s^{-1} in the range of 200−800 K and $k_t = 7.11 \times 10^{-23}T^{3.38} \exp(-1097/T)$ cm^3·molecule^{-1}·s^{-1} in the range of 800−3000 K, which are in close agreement with experimental data. The branching ratios of enol channels are consistent with the observation in low-pressure flames and hence the reaction mechanisms presented here provide valuable descriptions of enol formations in hydrocarbon combustion chemistry.

1. Introduction

Recently, enols, the unstable tautomers of aldehydes and ketones, have been found to be the intermediates in hydrocarbon combustion flames.[1,2] Enols were first postulated in 1880 by Erlenmeyer[3] as transient chemical intermediates, until 1976[4] the simplest enol, ethenol ($CH_2{=}CHOH$) was observed in a gas phase. Since then, enols have been the subject of numerous experimental and theoretical studies.[5−7] Now it is evident that they are present in substantial concentrations in a wide range of flames. In 2003, Cool et al.[2] observed the ethenol in a ethene-rich flame for the first time, and then Taatjes et al.[1] studied the ethenol, propenols, and butenols in a wide range of pure and mixed-fuel flames in 2005. The traditional hydrocarbon combustion chemistry models assume C_2H_4O molecules observed in flames as acetaldehyde or oxirane, but Taatjes et al.[1] discovered the ethenol kinetics in flames differing from those of the acetaldehyde tautomer. Consequently, Taatjes et al. proposed that there should be different mechanisms in the formation of ethenol and acetaldehyde tautomers, and the flame concentrations are the result of the competing effects of many reactions.[1] So theoretical studies are needed to explain the phenomena of enol formation and destruction. Most recently, Taatjes et al.[8] reported the mole fraction profiles of enols in combustion flames of rich ethene, allene, propene, butylenes, cyclopentene, etc., and proposed that the reaction of OH radical with ethene is the dominant source of ethenol in many hydrocarbon flames. However, from the mole fraction profile obtained from the propene-rich flame, the correlation between mole fractions of ethene and ethenol indicates that the reaction of OH + ethene is not the sole source of ethenol, so ethene is not the sole precursor, while the OH + $CH_3CH{=}CH_2$ reaction is still responsible for the formation of ethenol. So the investigation of the combustion chemistry mechanisms of the new reactions for enol production will be helpful to the development of the present hydrocarbon combustion chemistry models. This is just our motivation in carrying out the study of OH + propene reaction so as to elucidate the formation chemistry of ethenol and propenol in flames.

Reliable rate constants for the production of enols in an OH + propene reaction are not yet available. The overall kinetics of the reaction has been extensively studied experimentally,[9−17] but there are few measurements of the reaction products. Hoyermann and Sievert[18] measured the products of this reaction at low pressure and room temperature. They have noted several channels to get the products, such as the channel of producing methyl and C_2H_4O assigned as acetaldehyde, and the channel of producing H and C_3H_6O assigned as acetone. But the products are probably including enols. On the other hand, several theoretical studies have been reported for this system.[19−21] Alvarez-Idaboy et al.[20] have carried out ab initio calculations for the mechanism of OH + propene reaction at low pressure in inert atmosphere, just focusing on the reaction channels about the products of acetone, propionic aldehyde, formaldehyde, etc. However, the formations of ethenol and propenols, two possible important reactions, have been ignored. Szori et al.[21] have investigated the allylic H-abstraction mechanism in the reaction of the OH + propene system at lower temperature, but surprisingly the formation of enols has not been involved, and the kinetic comparisons with all of the reaction channels have not been well established either. Therefore, more details are

[†] College of Chemical Engineering.
[‡] College of Chemistry.

10.1021/jp808574g CCC: $40.75
Published on Web 02/20/2009

required for the descriptions of the formations and kinetic properties of enols in this reaction system. If the reaction of OH + propene is similar to the reaction of OH + ethene,[22] one may expect formation of ethenol and methyl radicals by C−C fission following addition to the central carbon. Factually, both formations of propen-2-ol by C−H fission following OH addition to the central carbon, and of 1-propenol following terminal addition, are thermodynamically possible,[23−27] analogous to the formation of ethenol in the reaction of OH with ethene. Holmes et al.[25] proposed that at the temperature above 1226 K the yield of enol decreases and ketene and methane are produced.

Accurate calculations of the electronic energies for radical structures are quite sensitive to the treatment of electron correlation. The thermochemical properties of enols including ethenol, propen-2-ol, propen-1-ol, etc., have been investigated by Tureček et al.,[26] and the results showed that the total energies for any species mentioned above differs greatly by means of different methods. So it is very important to determine which method is most suitable for the reaction involving enols. The reaction of OH + ethene has also been sufficiently studied by several groups[16,22,28−36] with ab initio calculations. Sekušak et al.,[29] Piqueras et al.,[31] Villà et al.,[32] and Sosa and Schlegel[34] have investigated the entrance barrier and the reaction enthalpy with respect to the size and quality of basis sets and the treatment of correction energies. Their results indicated that the entrance barrier height and enthalpy are very sensitive to the method employed. Sekušak et al.[29] found that the results agree best with the experimental results are obtained at the MP2/aug-cc-pVTZ//UMP2/6-311+G(2d,p) level of theory. Zhu et al.[22] investigated the entrance barrier and the reaction enthalpy of the process $OH + C_2H_4 + M \rightarrow C_2H_4OH + M$ at several levels of theory, including CCSD(T), G3, G2M(CC1), G3B3, and PMP2. Their results showed that values in good agreement with experimental values are obtained at the PMP2 level with the aug-cc-pVQZ basis set. On the other hand, Alvarez-Idaboy et al.[35] have investigated the reaction of OH addition to ethene with different methods, including PMP2, PMP4, and CCSD(T). They proposed that PMP2 with large basis sets up to aug-cc-pVTZ gave the best agreement between theoretical and experimental activation energies. Galano et al.[36] have investigated the reaction of OH with formic acid at several levels of theory, such as MP2, MP4, B3LYP, BHandHLYP, CCSD(T), and QCI. They proposed that the best results were obtained with the PMP2/6-311++G(2d,2p)//MP2/6-311++G(2d,2p). Obviously, the MP2 method is the best one to describe the OH addition reaction system, so the MP2 method is employed to calculate the reaction of OH radical with propene in this work.

On the basis of the reasons mentioned above, we carry out the theoretical investigations on the reaction channels, the rate constants, and the branching ratio of OH + propene system at different temperatures and pressures. Particular attention is paid to the formation of enols.

2. Computational Methods

The MP2 method with the cc-PVTZ basis set is employed to fully optimize the equilibrium geometries of the reactants, van der Waals prereaction complex, intermediates, transition states (TSs), and products. The zero-point vibrational energy corrections (ZPE) calculated at this level have been scaled by a standard factor of 0.95 as suggested by Scott and Radom.[37] In addition, vibration frequency calculations are also carried out to confirm the existence of transition states with one and only one imaginary frequency. The intrinsic reaction coordinate (IRC) calculations are carried out to confirm that the transition states are connecting the right minima between a specific pair of stationary points. Single-point energies of all species are obtained by the PMP2 method with large basis set aug-cc-PVQZ. CCSD(T)/6-311+G(3df,2p), B3LYP, CCSD(T) with cc-pV*X*Z extrapolated to complete the basis set (CBS) limit[38] calculations are also carried out for some important reaction channels for comparison. All of the electronic structure calculations were performed with the Gaussian 03 program.[39]

For unimolecular reactions, we employ Rice−Ramsperger−Kassel−Marcus (RRKM) theory[40] and master equation calculations to compute the pressure- and temperature-dependent rate constants. Several packages developed based on RRKM theory are available, for example, the UNIMOL program,[41] the ChemRate program,[42] and the Variflex program.[43] Among them, Variflex has the most sophisticated and realistic treatment of loose transition states found in barrierless association reactions and unimolecular reactions. In this work, we employed the Variflex code to perform the rate constant calculations. Reactions with loose transition states were treated using variable reaction coordinate-transition state theory (VRC-TST) formalism.[44,45] Reactions with tight transition states were treated using a canonical nonvariational transition state theory.[45]

3. Results and Discussion

The optimized geometries of the prereaction complex, intermediates, transition states, and product are shown in Figure 1. Energies of the species in the entrance channel of this reaction system are listed in Table 1. Although in general the CCSD(T) method yields more reliable results for transition states, here MP2 seems to predict better energies when compared with the data from the literature.[20,35,46]

Meanwhile, we calculated the reaction enthalpies ($\Delta_r H_0°$) for three different channels at different levels. The predicted reaction enthalpies determined by different methods including PMP2/aug-cc-PVQZ, CCSD(T)/ 6-311+G(3df,2p), and CCSD(T) with cc-pV*X*Z extrapolated to complete basis set (CBS) limit[38] are listed in Table 2. The CBS extrapolation equation at the CCSD(T) level used here is provided by Huh[38] with the cc-PV*X*Z basis sets

$$E^{\mathrm{corr}}(\infty) = E^{\mathrm{corr}}(X) + A/(X + 1/2)^3 \qquad (1)$$

($X = 2, 3$) for D-T extrapolation.

The predicted values are compared with the experimental reaction enthalpies using the available experimental heats of formation.[49−53] The deviations between the experiment and the predicted reaction enthalpy $\Delta\Delta_r H_0°$ obtained with different methods are also listed in Table 2. It is shown that for$OH + C_3H_6 \rightarrow CH_2CHOH + CH_3$, the two CCSD(T) methods are slightly better than the PMP2 method, but for the other two reactions,$OH + C_3H_6 \rightarrow CH_3CH_2 + CH_2O$ and $OH + C_3H_6 \rightarrow CH_3CHCHOH + H$, the PMP2 method is much better than the CCSD(T) methods. The results by the CCSD(T) method deviate considerably from the experimental ones, the $\Delta\Delta_r H_0°$ for the reaction $OH + C_3H_6 \rightarrow CH_3CHCHOH + H$ being 5.06 kcal/mol with the CCSD(T)/6-311+G(3df,2p) method and 4.96 kcal/mol with the CCSD(T)/CBS method. The results obtained at the PMP2 level with a large basis set (aug-cc-PVQZ) are in reasonable agreement with the experiment, which are similar to those of the $OH + C_2H_4$ system calculated by Zhu et al.[22] Therefore, the relative energies in the following are calculated at the PMP2/aug-cc-PVQZ//MP2/cc-PVTZ level, which are used for the rate constant calculation.

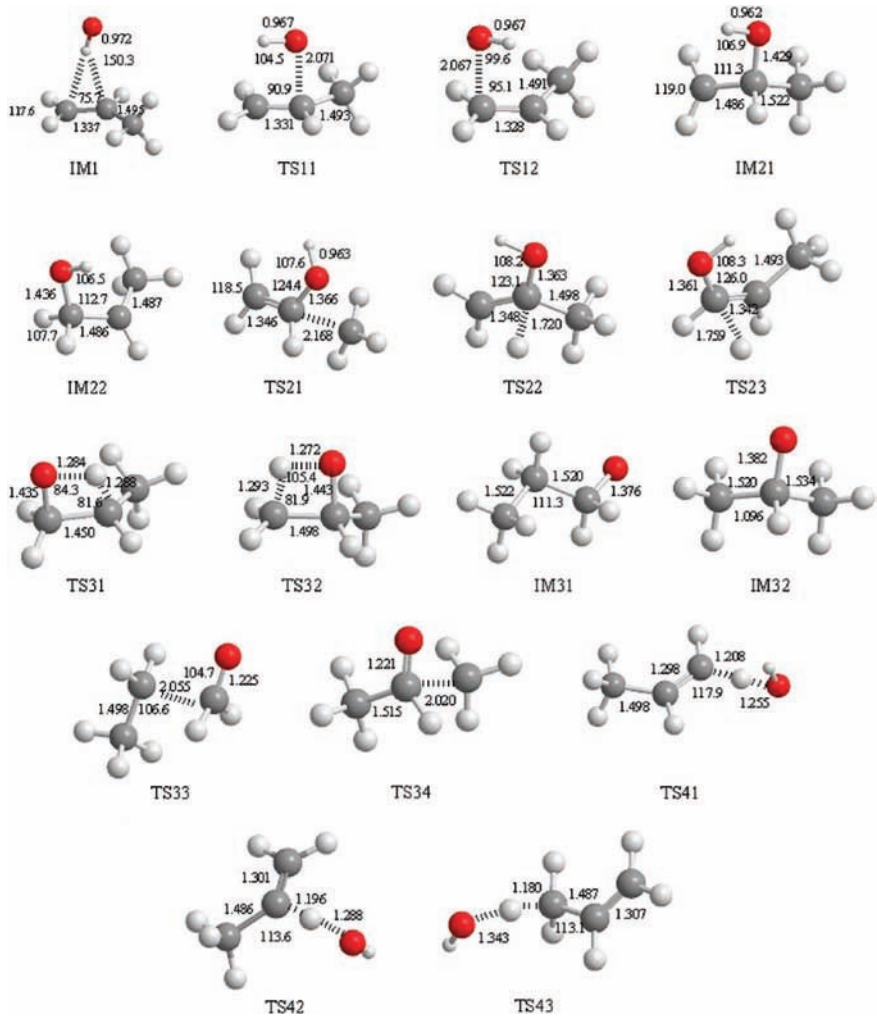

Figure 1. Optimized geometries of the prereaction complex, intermediates and transition states involved in the reaction of HO + propene at the MP2/cc-PVTZ level. The bond lengths are given in angstroms, and the angles are given in degrees.

TABLE 1: Comparison of Energies (kcal/mol) Relative to Reactants for the Species in the Entrance Channel of This Reaction System

species	E_{PMP2}	$E_{CCSD(T)}$	ref 20[a]
CH_3CHCH_2 + OH	0	0	0.0
IM1	−2.6	−2.5	−2.9
TS11	−1.4	0.2	−2.1 [−2.06]
TS12	−1.1	0.3	−1.7 (−1.00)
IM21	−32.3	−27.0	−33.2
IM22	−30.6	−26.1	−30.5

[a] The value in brackets is proposed by Cvetanovic,[46] the value in parentheses is proposed by Alvarez-Idaboy et al.[35]

3.1. Potential Energy Profile and Reaction Mechanism. Electrophilic addition to the CC double bond is a crucial mode of OH radical attack on propene. In addition, the H-abstraction mode may play an important role in the overall kinetics. We rely on chemical intuition in considering the probable reaction pathways. According to the sites of the interaction between OH radical and the propene, three branches are selected: central addition (Scheme 1), terminal addition (Scheme 2), and direct H-abstraction (Scheme 3).

The global potential energy profile at the PMP2/aug-cc-PVQZ//MP2/cc-PVTZ level is schematically shown in Figures 2 and 3. Factually, some structures in Figure 1 have more than one conformation, but here we use the most stable one for our purpose, with the implicit assumption that conformational

TABLE 2: Reaction Enthalpies ($\Delta_rH_0°$) of Three Different Channels Predicted at the Different Levels of Theory at 0 K in Units of kcal/mol, the Geometries Are All Obtained at the MP2/cc-PVTZ Level

OH + C_3H_6 → CH_2CHOH + CH_3	$\Delta_rH_0°$	$\Delta\Delta_rH_0°$
PMP2/aug-cc-PVQZ	−11.9	−4.0 ± 2.0
CCSD(T)/6-311+G(3df,2p)	−8.9	−1.0 ± 2.0
CCSD(T)/CBS[38]	−9.3	−1.4 ±2.0
exptl[a]	−7.9 ± 2.0	
OH + C_3H_6 → $CH_3CHCHOH$ + H	$\Delta_rH_0°$	$\Delta\Delta_rH_0°$
PMP2/aug-cc-PVQZ	−4.6	−1.34± 0.007
CCSD(T)/6-311+G(3df,2p)	1.8	5.06 ± 0.007
CCSD(T)/CBS[38]	1.7	4.96 ± 0.007
exptl[a]	−3.26 ± 0.007	
OH + C_3H_6 → CH_3CH_2 + CH_2O	$\Delta_rH_0°$	$\Delta\Delta_rH_0°$
PMP2/aug-cc-PVQZ	−14.1	−1.04 ± 0.493
CCSD(T)/6-311+G(3df,2p)	−12.4	
CCSD(T)/CBS[38]	−10.3	0.66 ± 0.493
exptl[a]	−13.06 ± 0.493	2.76 ±0.493

[a] The heats of formation from literature: $\Delta_fH_0°$(OH) = 8.86 ± 0.007 kcal/mol (ref 47), $\Delta_fH_0°(CH_3)$ = 35.86 ± 0.07 kcal/mol (ref 48), $\Delta_fH_0°$ (H) = 52.1 kcal/mol, $\Delta_fH_0°(CH_2O)$ = −27.7 kcal/mol (ref 49); $\Delta_fH_0°(C_3H_6)$ = 4.9 kcal/mol (ref 50); $\Delta_fH_0°(CH_2CHOH)$ = −30.0 ± 2.0 kcal/mol (ref 51); $\Delta_fH_0°(CH_3CH_2)$ = 28.4 ± 0.5 kcal/mol (ref 52); $\Delta_fH_0°(CH_3CHCHOH)$ = −41.6 kcal/mol (ref 53).

SCHEME 1

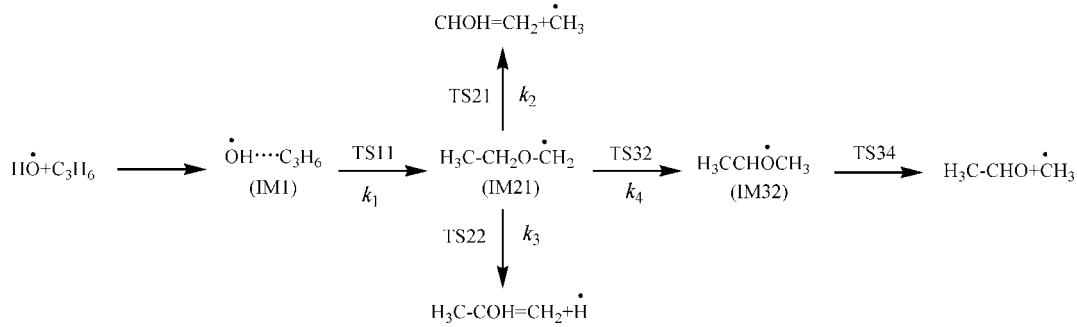

SCHEME 2

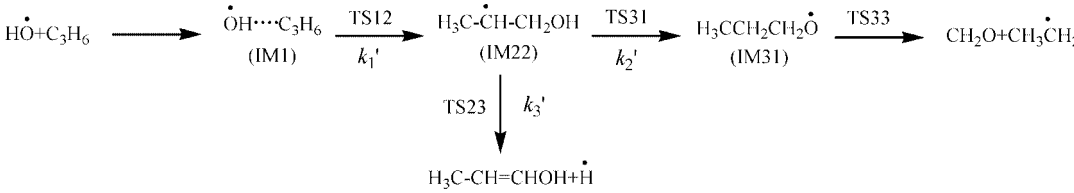

SCHEME 3

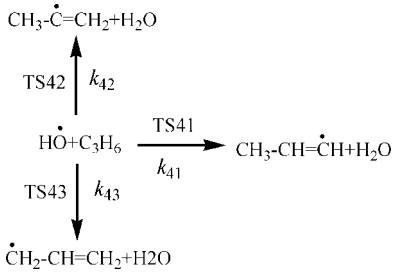

changes are rapid relative to chemical reactions and are thus best treated as internal rotations. In the following, the elementary reactions involved in each channel will be described in detail.

3.1.1. Association/Dissociation Reaction Processes. The interaction between the hydrogen atom of the OH and the electron density of the double bond of propene forms a prereaction van der Waals complex (IM1) in which the OH radical is almost perpendicular to the CC double bond, with the positively charged H atom pointing toward the double bond. The addition of the OH radical can occur at both carbon atoms of the double bond. When the OH radical attacks the central C of propene, the intermediate IM21 ($CH_3-CHOH-CH_2$) is formed via the transition state TS11 lying below the reactant by 1.4 kcal/mol with a potential energy barrier of 1.2 kcal/mol, as shown in Scheme 1. On the other hand, if the OH radical is added to the terminal C of propene in the double bond, the intermediate IM22 ($CH_3-CH-CH_2OH$) is formed via TS12 lying below the reactant by 1.1 kcal/mol with a potential energy barrier of 1.5 kcal/mol, as shown in Scheme 2. The geometries of TS11 and TS12 are illustrated in Figure 1, and the relative energies of TS11 and TS12 by taking the energies of reactants as zero are given in Table 2. Normally, the strong site selectivity results from a larger positive barrier height for the addition of OH radical at the central C; however, in this case, the 1.2 kcal/mol barrier height is obtained, which apparently could not prevent the addition. So the site selectivity of the addition of OH radical is weak. Furthermore, after TS11 and TS12, two stable adducts, IM21 and IM22, are formed, which have the relative energies of −32.3 and −30.6 kcal/mol, respectively.

Three decomposition pathways for IM21 and two for IM22 have been investigated, and the energies are shown in Figure 2. From the structure of TS11 (Figure 1), the OH radical group in this case rotates and the O atom moves toward one terminal C atom of the double bond to form a C−O bond, and then the stable intermediate IM21 is produced. Alternatively, in the structure of TS12, the OH radical group rotates so that the O atom moves toward the other central C atom of the double bond to form a C−O bond. This finally leads to the stable intermediate IM22. Three decomposition channels of IM21, as shown in Scheme 1 were taken into consideration. In the first pathway, IM21 eliminates a CH_3 radical directly to form the products CH_2═CHOH and CH_3 radical via transition state TS21 lying bellow the reactants by 1.7 kcal/mol with the potential energy barrier of 30.6 kcal/mol. In the second channel, the H atom bonded to the central C of IM21 is eliminated to form the products CH_3COH═CH_2 and H via the transition state TS22 with the potential energy barrier 31.3 kcal/mol. In the third channel, the H atom in the OH radical group of IM21 migrates to the terminal C to form IM32 (CH_3CHOCH_3) through a four-member-ring (2C−O−H−1C) transition state TS32 with a potential energy barrier of 33.1 kcal/mol. Then IM32 can directly dissociate to the products CH_3CHO and CH_3 radical via TS34. The relative energies for the reactants of IM32 and TS34 are −22.5 and −11.6 kcal/mol, respectively, with the potential energy barrier 10.9 kcal/mol. As for the decomposition of IM22 shown in Scheme 2, two separate channels were taken into account. In the first pathway, IM22 eliminates an H atom to form the products CH_3CH═CHOH and H atom via the transition state TS23 with the potential energy barrier of 31.9 kcal/mol. The other channel involves migration of the H atom. The H atom in the OH radical group of IM22 shifts to the central C to form IM31 via a four-member-ring (1C−O−H−2C) transition state TS31 with the potential energy barrier of 34.3 kcal/mol. Then IM31 can directly dissociate to the products CH_3CH_2 and HCHO through the transition state TS33 with the potential energy barrier of 11.4 kcal/mol.

Besides these investigations, we also studied the intramolecular elimination of the H atom and OH radical group to form H_2O; however, they contribute negligibly to the overall rate constant in comparison with the other channels studied in this paper because of their higher activation barriers. So this type of reaction is not taken into consideration in the following investigations.

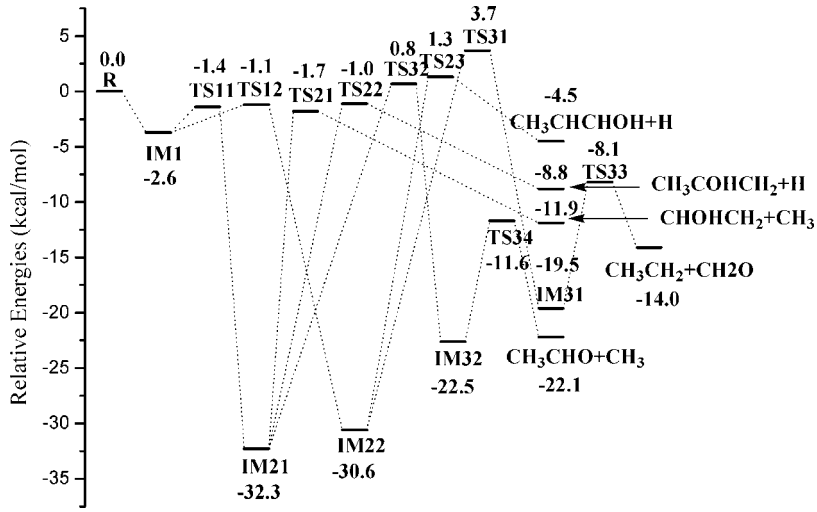

Figure 2. Potential energy diagram for association/dissociation branches of OH + propene reaction at the PMP2/ aug-cc-PVQZ//MP2/cc-PVTZ level.

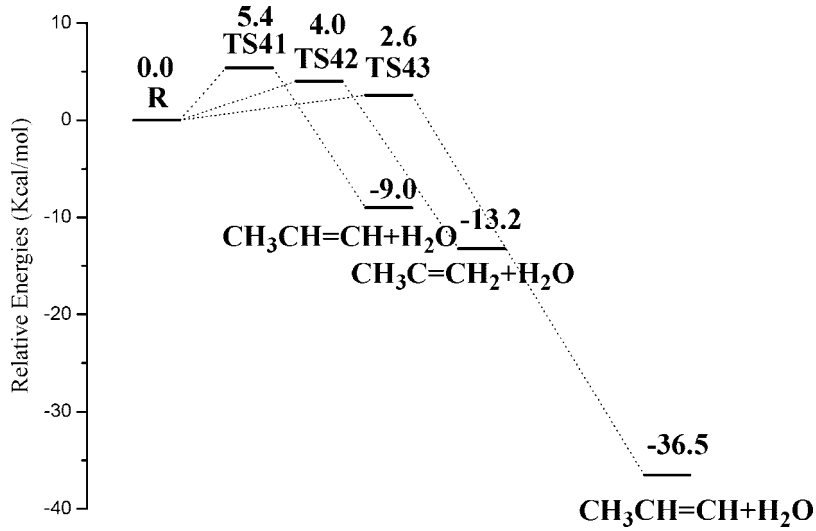

Figure 3. Potential energy diagram for direct H-abstraction branches of OH + propene reaction at the PMP2/ aug-cc-PVQZ//MP2/cc-PVTZ level.

3.1.2. Direct H-atom Abstraction Process. From Scheme 3, it can be seen that there are three direct H abstraction channels in which OH attacks different types of H atom of propene to produce H_2O and other products. In these processes, no stationary van der Waals complex between OH and $CH_3-CH=CH_2$ was formed. All of the transition state structures are shown in Figure 1. The first channel to the products $CH_3-CH=CH$ and H_2O has a potential barrier of 5.4 kcal/mol via the transition state TS41. It has only one imaginary vibrational frequency of $i2063$ cm^{-1}, whose vibrational vector corresponds to the H-abstraction motion (Table 3). The second channel corresponds to the H abstraction by OH radical from the middle C of $CH_3-CH=CH_2$, which produces $CH_3-C=CH_2$ and H_2O via the transition state TS42 with a potential barrier of 4.0 kcal/mol. The third channel for products $CH_2-CH=CH_2$ and H_2O has the barrier of 2.7 kcal/mol via the transition state TS43. Apparently, the abstraction of the H atom from the CH_3 group in $CH_3-CH=CH_2$ is relatively easier.

3.2. Rate Constants and Product Branching Ratios. Another major goal of this study lies in the prediction of the reaction rate constants. The rate constants for all product channels presented above have been calculated using variational transition state theory and RRKM theory with Variflex code.[43] For the barrierless processes, the number of a variational transition quantum states, $N^{\dagger}_{EJ}$, was given by the variationally determined minimum in $N_{EJ}(R)$, as a function of the bond length along the reaction coordinate R, which was evaluated according to the variable reaction coordinate flexible transition state theory.[55−58] The basis of these methods involves a separation of the vibrational modes into conserved and transitional modes. With this separation, one can evaluate the number of states by Monte Carlo integration for the convolution of the sum of vibrational quantum states for the conserved modes and the classical phase space density of states for the transitional modes.[55−58] In this work, the configuration number of Monte Carlo integration is 5000. To facilitate the use of the reaction rate constants for chemical kinetics modeling, we fitted all rate constants in the temperature range from 200 to 3000 K to a modified three-parameter Arrhenius expression

$$k(T) = AT^n \exp\left(-\frac{E_b}{RT}\right) \quad (2)$$

This formulation leads to a better fit than the ordinary Arrhenius expression, but the parameters may have little physical interpretation.

TABLE 3: Vibrational Frequencies and Rotational Constants (*B*) at the MP2/cc-PVTZ Level for the Main Species in the C_3H_6 +OH Reaction System

species	*B*/MHz	frequencies[a] (cm^{-1})
OH		3820
C_3H_6	46660, 9376, 8199	196, 401, 562, 892, 896, 899, 983, 1020, 1138, 1261, 1340, 1388, 1421, 1434, 1622, 2915, 2985, 3006, 3019, 3032, 3114
IM1	8235, 3715, 2826	55, 69, 120, 202, 305, 373, 401, 576, 895, 900, 905, 992, 1025, 1140, 1262, 1342, 1388, 1421, 1433, 1613, 2918, 2992, 3008, 3017, 3031, 3113, 3540
TS11	8759, 6903, 4452	497*i*, 118, 182, 224, 275, 408, 605, 713, 900, 911, 949, 1010, 1064, 1154, 1278, 1338, 1399, 1418, 1435, 1640, 2930, 3011, 3036, 3038, 3069, 3136, 3618
TS12	12415, 4764, 3966	498*i*, 104, 158, 193, 263, 410, 669, 722, 903, 910, 997, 1032, 1060, 1150, 1276, 1342, 1397, 1418, 1433, 1656, 2920, 2990, 3021, 3043, 3054, 3147, 3619
IM21	8968, 8597, 5040	174, 240, 316, 323, 396, 451, 544, 813, 885, 929, 1006, 1103, 1111, 1224, 1313, 1318, 1335, 1403, 1425, 1437, 2887, 2927, 3019, 3023, 3041, 3156, 3652
IM22	15681, 5108, 4343	97, 134, 261, 314, 388, 549, 847, 871, 942, 975, 1077, 1106, 1158, 1305, 1316, 1345, 1355, 1423, 1429, 1437, 2876, 2891, 2938, 2969, 3017, 3076, 3651
TS21	8808, 6610, 4312	764*i*, 131, 205, 280, 353, 459, 544, 574, 581, 761, 854, 916, 991, 1076, 1251, 1288, 1375, 1378, 1387, 1533, 2974, 3045, 3087, 3137, 3141, 3154, 3644
TS22	9491, 8619, 4960	1342*i*, 221, 372, 402, 442, 538, 574, 618, 679, 815, 853, 944, 982, 1028, 1157, 1312, 1346, 1399, 1416, 1432, 1574, 2938, 3023, 3049, 3053, 3157, 3637
TS23	15650, 5449, 4367	1257*i*, 90, 243, 279, 363, 546, 595, 641, 746, 900, 1000, 1013, 1049, 1081, 1186, 1289, 1341, 1374, 1424, 1439, 1593, 2899, 2964, 3006, 3084, 3100, 3651
TS31	17739, 5064, 4741	2095*i*, 162, 221, 353, 658, 725, 855, 900, 960, 1031, 1096, 1106, 1120, 1143, 1241, 1295, 1347, 1429, 1435, 1467, 2007, 2915, 2937, 2992, 2999, 3016, 3033
TS32	11557, 7382, 5305	2130*i*, 239, 318, 340, 436, 684, 828, 863, 885, 973, 1034, 1083, 1116, 1154, 1227, 1322, 1351, 1370, 1425, 1436, 2001, 2921, 2954, 3002, 3009, 3016, 3120
IM31	27936, 3969, 3712	122, 222, 254, 418, 534, 743, 856, 926, 1006, 1025, 1084, 1185, 1240, 1261, 1328, 1341, 1347, 1429, 1442, 1446, 2837, 2888, 2919, 2938, 2982, 3002, 3012
IM32	9618, 8116, 5078	194, 243, 329, 348, 431, 800, 871, 887, 898, 1032, 1089, 1126, 1255, 1296, 1316, 1337, 1417, 1425, 1431, 1451, 2885, 2924, 2933, 3012, 3019, 3026, 3033
TS33	22989, 3667, 3372	521*i*, 79, 164, 204, 335, 585, 675, 796, 825, 948, 1039, 1161, 1166, 1212, 1337, 1422, 1423, 1432, 1460, 1663, 2764, 2822, 2908, 2984, 3021, 3031, 3131
TS34	9036, 7163, 4568	662*i*, 145, 201, 251, 359, 474, 605, 635, 821, 875, 917, 1052, 1095, 1313, 1340, 1369, 1387, 1413, 1419, 1619, 2762, 2926, 2984, 3011, 3040, 3151, 3164
TS41	32271, 2633, 2501	2063*i*, 105, 130, 174, 223, 347, 517, 752, 840, 888, 917, 994, 1076, 1111, 1206, 1272, 1337, 1350, 1423, 1430, 2079, 2924, 2999, 3020, 3044, 3084, 3627
TS42	9131, 4619, 3164	1867*i*, 101, 143, 174, 219, 361, 531, 712, 836, 902, 921, 993, 1037, 1098, 1176, 1332, 1361, 1386, 1414, 1427, 2111, 2921, 3008, 3010, 3025, 3114, 3622
TS43	18590, 2901, 2731	1639*i*, 58, 81, 110, 351, 392, 604, 706, 850, 910, 928, 1016, 1070, 1092, 1144, 1233, 1299, 1368, 1390, 1418, 2077, 2963, 3029, 3040, 3059, 3120, 3617

[a] Values are scaled by 0.95. *i* denotes the imaginary frequency.

To carry out the variational transition-state rate calculation for the barrierless association process of HO + C_3H_6 → HOC_3H_6, the Morse potential function $E(R) = D_e[1 - e^{-\beta(R-R_e)}]^2$ was used to represent the potential energy along the minimum energy path of each individual reaction coordinate. In the above equation D_e is the bond energy excluding zero-point vibrational energies for an association reaction, R represents the reaction coordinate (i.e., the distance between the two bonding atoms; the H−C bond in the present case), and R_e is the equilibrium value of R at the stable intermediate structure. The potential function was computed by scanning the H−C bond from 2.4 to 8.4 Å with step size of 0.15 Å, with other geometric parameters being fully optimized. The result of simulation is shown in Figure 4. The computed energies could be fitted reasonable to the Morse potential function with the parameters $D_e = 3.2$ kcal/mol and $\beta = 1.018$ $Å^{-1}$. Table 3 lists the rotational constants and harmonic frequencies that were used to calculate rate constants. The *E*/*J* (energy *E* and total angular momentum *J*) resolved variable reaction coordinate transition state theory (VRC-TST) formalism[59] and the master equation formalism[60] implemented in the Variflex code were used to evaluate the TS partition function and the pressure dependence. An energy grain size of 100 cm^{-1} was used to achieve convergence in the integration over the energy range. The grain size provides numerically converged results in the temperature studied with the energy range spanning from −11293.40 to 68606.60 cm^{-1} and from −10698.90 to 69201.10 cm^{-1} for the processes shown in Scheme 1 and Scheme 2, respectively. The total angular momentum *J* covered the range from 1 to 250 in steps of 10 for the *E*- and *J*-resolved calculations.

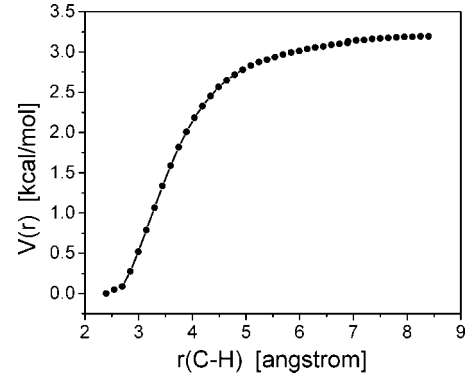

Figure 4. Morse curve for the association process HO + C_3H_6 → HOC_3H_6. Points are computed at the MP2/cc-PVTZ level of theory, and the solid curve is the fitted Morse function.

The behavior of energy transfer is assumed to be induced by a weak molecular collision, and the frequency of collision was derived from the Lennard-Jones (L-J) pairwise potential parameters of N_2 ($\sigma(N_2) = 3.798$ Å, $\varepsilon/k_B(N_2) = 71.4$ K)[61] and *n*-C_3H_7OH (σ(*n*-C_3H_7OH) = 4.549 Å, ε/k_B(*n*-C_3H_7OH) = 576.7 K).[61] These values were employed for the evaluation of the L-J

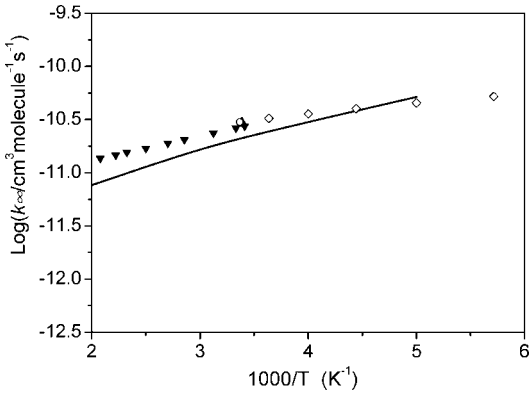

Figure 5. The predicted total rate constant at the high-pressure limit (solid line) and experimental data reported at the high-pressure limit from (▲) ref 12, (◇) ref 13, (▼) ref 14, and (○) ref 17.

parameters for each collision pair using the approximations $\sigma_{12} = (\sigma_1 + \sigma_2)/2$ and $\varepsilon_{12} = (\varepsilon_1\varepsilon_2)^{1/2}$. $P(E \rightarrow E')$ is the probability that a complex with an energy between E and $E + dE$ will be transferred by a collision to a state with an energy between E' and $E' + dE'$. The energy transfer rate constants were described on the basis of the "single exponential down" expression

$$P(E \rightarrow E') \propto \exp\left(-\frac{E - E'}{\langle \Delta E_d \rangle}\right) \qquad E > E' \tag{3}$$

where $\langle \Delta E_d \rangle$ is the average energy loss per collision of the active component with a bath gas molecule, whose value depends on the nature of the collider gas, in this case of N_2. Although, the experimental $\langle \Delta E_d \rangle$ data for most of the molecules are not available, these values can be obtained by fitting the experimental pressure-dependent rate constants with the calculated values using the exponential down model in the solution of the Master equation. For example, by fitting the falloff experimental data, the $\langle \Delta E_d \rangle$ values for the deactivations of different species in N_2, the values are 210 cm^{-1},[62] 250 cm^{-1},[63] and 400 cm^{-1},[64] and we adopted the $\langle \Delta E_d \rangle$ value of 200 cm^{-1} for the energy transfer in N_2 in this work as suggested by Zhu.[65] The Morse potential with the parameters above-mentioned, the Lennard-Jones pairwise potential, and the anisotropic potential (a potential anisotropy form assuming a bonding potential which is cylindrically symmetric with respect to each fragment) are added together to form the final potential for the variational rate constant calculation by the Variflex code. The number of the states for the tight transition states is evaluated according to the rigid-rotor harmonic-oscillator assumption employed in the Variflex code.[66] The quantum tunneling effects were included in the related cases with the Eckart tunneling model.[67]

Our calculation indicates that in the whole temperature range at high pressures the contribution of the rate constant is dominated by the reactions forming stable IM21 and IM22. However, even at 650 K and at atmospheric pressure, 76.8% of the total rate constant is contributed from the electrophilic addition channels. The high-pressure limit for the rate constant (i.e., including the direct H abstract processes) of propene reaction with OH is plotted in Figure 5, along with data (reported in literatures) at this limit. Transition state input, USTTSP,[68] in Variflex has been used to calculate the entrance channel forming the stable adducts IM21 and IM22, in which the multiple reflections[68,69] are taken into consideration. Calculation of this reaction process without multiple reflections is also carried out. Comparison of the total rate constants with and without multiple reflections is shown in Figure S1 in the Supporting Information together with the experimental values. We can get that multiple reflections above the IM1 complex well reduce the rate constant effectively in the lower temperature range (200−400 K), but the effect gradually decreases in higher temperature range (500−3000 K). For example, the ratio of total rate constants with/without multiple reflections is 0.50 at 300 K and 0.86 at 400 K. When the temperature is large than 500 K, the two values are almost the same. The tendency of the multiple reflections effection in this reaction system is almost the same as that reported in Lin's work[70] in which the same prereaction well was taken into account. On comparisons of our calculated high-pressure limit for the total rate constant with the experimental data reported at the high-pressure limit, we find a reasonable agreement between our results and the low-temperature experimental data of Vakhtin et al.[13] and are slightly lower than the measurements of Klein et al.,[12] Tully et al.,[14] and Zellner et al.,[17] at somewhat higher temperatures.

The temperature dependence of the addition rate constants for IM21 and IM22 are plotted in Figure 6a and Figure 6b, respectively, at several pressures. As expected of a barrierless addition processes, both of the two rate constants show reverse temperature dependence. The rate constants of the two channels show pressure independence at the temperature range 200−500 K; this is because the energy barriers for isomerization are highly relative to the reactants and the complexes of IM21 and IM22 are virtually the only stabilized ones in this temperature range at the pressures investigated. But at the higher temperature range 500−3000 K the rate constants show a strong pressure dependence. On the other hand, the rate constants of these two channels show a reverse temperature dependence when the temperature is above 800 K. This is because the addition channels become unimportant due to the extremely rapid decomposition rate of OH−propene adducts IM21 and IM22 back to reactants at this higher temperature range. This tendency is consistent with the result of the analogical process in the reaction of OH with ethene calculated by Senosiain et al.[16] From the results of Senosiain et al.[16] and us, it can be concluded that the rate constants of the barrierless addition processes in this typical radical−molecule reaction show negative temperature dependence. Meanwhile, the multiple reflections[68,69] of these two channels have also been tested. For the channel obtaining IM21, the results show that the effect is significant at low temperatures, such as at 200 and 300 K, and the high pressure limit rate constants without multiple reflections are around 7 and 2 times higher than those with reflections, respectively. However, at higher temperatures (over 500 K), the effects are negligible. The results are similar to those of the OH + C_2H_4 system.[22] The channel obtaining IM22 has almost the same tendency.

The total rate constants at high temperatures are plotted in Figure 7 along with selected data from experiments and the recommendations. It can be seen that the experimental values from Smith et al.[10] and the recommended values at higher temperature range (960 K < T < 1210 K) from Atkinson[54] are close to the high pressure limit. Given the high precision of Smith's experiments, we decided to adjust the energy barrier by lowering the energies of transition states TS11 and TS12 by 1.0 kcal/mol. It should be mentioned that such an adjustment is well within the estimated accuracy (≈kcal/mol) of the theoretical methods. Rate constants at the high pressure limit (after this adjustment) are in reasonable agreement with the experimental values from the Smith[10] and the Atkinson[54] recommendations.

Rate constants for direct hydrogen abstraction from propene by OH radical are shown in Figure 8. These processes are

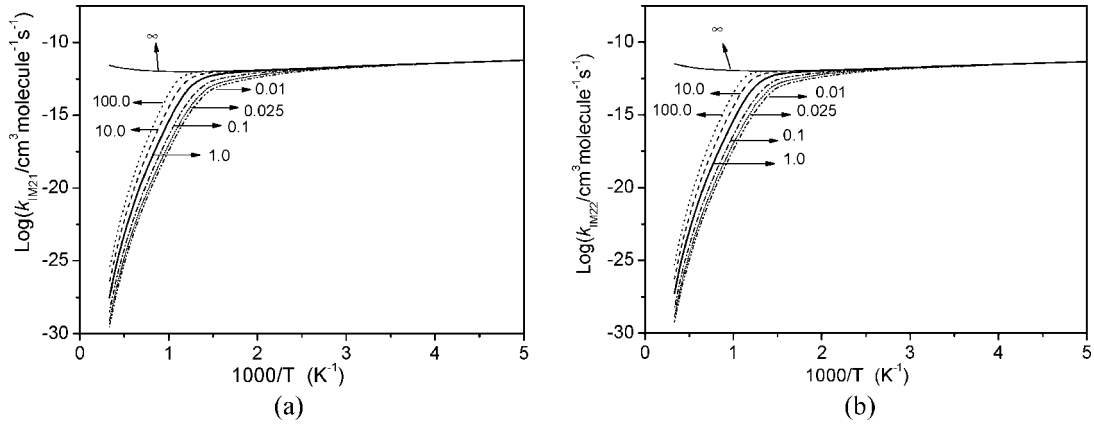

Figure 6. Predicted rate constants with multiple reflection correction for the addition reactions obtaining IM21 (a) and IM22 (b) at several pressures (in unit of atm) of N_2 diluent.

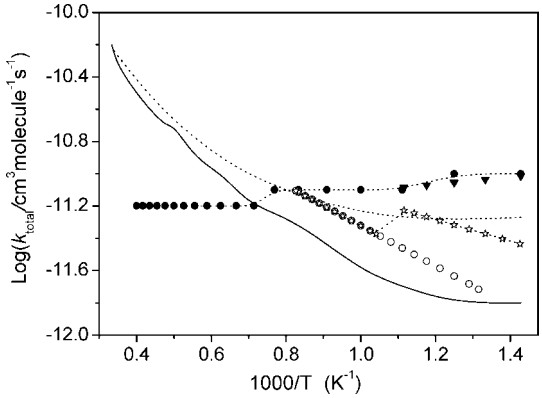

Figure 7. Total rate constants with multiple reflection corection at high temperatures. Also shown are experimental data and the recommended data: ○, ref 10; ▼, ref 14; ☆, ref 54; ●, ref 71. The solid line shows the predicted values at 0.01 atm, and the dotted line shows the predicted values at high pressure limit.

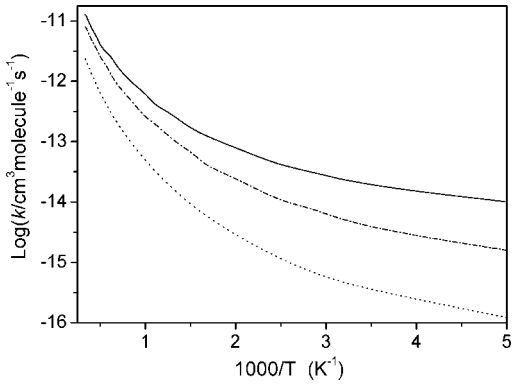

Figure 8. Rate constants for direct hydrogen abstraction processes. The dotted line shows the process obtaining $CH_3CHCH + H_2O$, the dash-dotted line shows the process obtaining $CH_3CCH_2 + H_2O$, and the solid line shows the process of $CH_2CHCH_2 + H_2O$.

pressure independent and are dominant at low pressures and/or high temperatures. From Figure 8 we can get that the process obtaining $CH_2CHCH_2 + H_2O$ is much more favored over the other two competitive channels. This is because the lower potential energy barrier of this channel and its product CH_2CHCH_2 is much more stable than the other two products.

Comparison of total rate constants calculated at several pressures with available experimental and recommended data[10−14,54,67] is given in Figure 9. In this process the predicted total rate constant represents the sum of the 11 channel rate

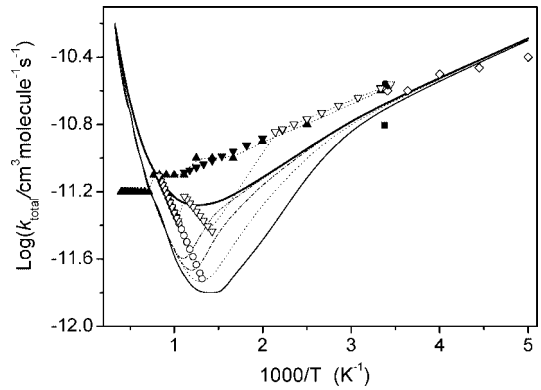

Figure 9. Comparision of predicted total rate constants with multiple reflection correction at several pressures with experimental data. The lines are our predict values at different pressures: solid thin line at 0.01 atm, the dotted line at 0.1 atm, the dash dotted line at 1 atm, the dash dotted dotted line at 10 atm, and the solid dark line at the high pressure limit. The symbols are the experimental values from different references: ○, ref 10; ◇, ref 11; ●, ref 12; ■, ref 13; ▼, ref 14; ▲, ref 71; ▽, ref 54.

TABLE 4: Comparison of the Total Rate Constants (in units of cm^3 molecule^{-1} s^{-1}) Obtained by the CCSD(T) Method with the Other Available Values at 1 atm

T	CCSD(T)	experimental or recommended values
300	6.74×10^{-13}	1.56×10^{-11},[13] 2.63×10^{-11},[14] 2.60×10^{-11},[54] 2.51×10^{-11} [71]
400	6.48×10^{-13}	1.7×10^{-11},[14] 1.71×10^{-11},[54] 1.58×10^{-11}[71]
500	6.46×10^{-13}	1.31×10^{-11},[14] 1.26×10^{-11} [71]
700	5.24×10^{-13}	9.69×10^{-12},[14] 3.67×10^{-12},[54] 1.00×10^{-11} [71]
800	4.76×10^{-13}	2.32×10^{-12},[10] 8.82×10^{-12},[14] 4.82×10^{-12},[54] 1.0×10^{-11} [71]

constants. From Figure 9, we can see that our predicted total rate constants decrease with the temperature increasing in the low temperature range (200 K < T < 800 K) and increase with the temperature increasing in the high temperature range (800 K < T < 3000 K). The marked change on activation energy reflects a change of the dominant reaction pathway, from the addition channels at temperatures below 800 K to the others including hydrogen abstraction channels above 1000 K. This typical phenomenon is also proposed by Senosiain et al.[16] in the OH with C_2H_4 reaction system. In addition, adjustment of the activation barriers of TS11 and TS12 mentioned above is also taken into consideration. Meanwhile, the effects of internal rotation of TS11 and TS12 on the total rate and product yields

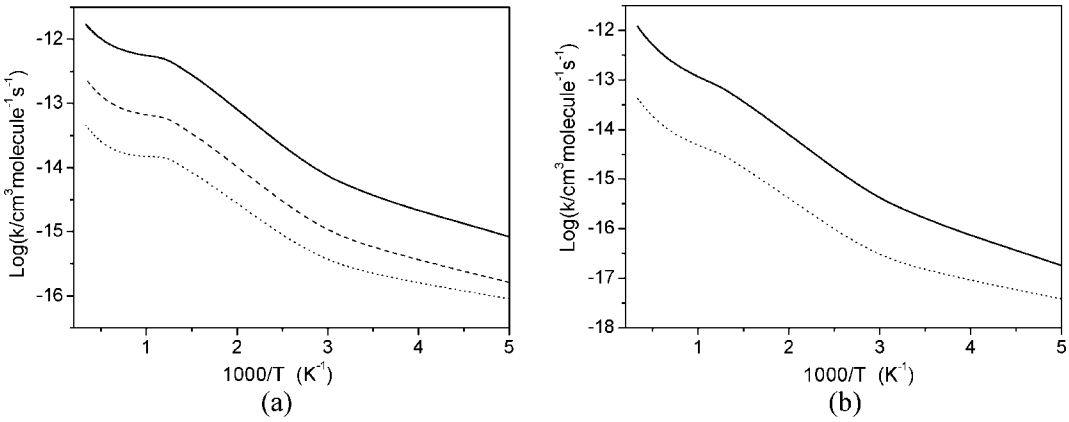

Figure 10. Rate constants of the competing channels. 760 Torr in N_2. The lines represent as: (a) The rate constants for products $CH_2CHOH + CH_3$ (k_2) (solid line), $CH_3COHCH_2 + H$ (k_3) (dashed line), and $CH_3CHO + CH_3$ (k_4) (dotted line). (b) The rate constants for products $CH_3CHCHOH + H$(k_3') (solid line), and $CH_2O + CH_3CH_2$ (k_2') (dotted line).

are also tested. The total rate constants after adjustment (1.0 kcal/mol) are in reasonable agreement with the experimental values from Smith,[10] Spangenberg,[11] and Atkinson.[54] On the other hand, we have carried out the CCSD(T)/cc-pVTZ//B3LYP/6-311G(3df,2p) calculations to test how the kinetics results will be affected by different methods. Comparison of the results in the lower temperature range (T < 900 K) obtained by the CCSD(T) method with the available recommended and experimental values is shown in Table 4. The total rate constants obtained by the CCSD(T) method appear to be 2 orders of magnitude lower than the data available for this temperature range. As a pertubation theory, MP2 sometimes overestimates the correlation effects. In the present case, however, the rate constants by MP2 are closer to the experimental values than the CCSD(T) results, due to a possible cancelation of errors. Although the CCSD(T) method is believed the more reliable method for the kinetic calculations, MP2 is found to be superior to CCSD(T) in this case.

Ethenol and propen-2-ol are formed by CH_3 and H eliminations from 2-hydroxypropyl radical, respectively, as shown in Scheme 1. The two processes are competitive, also with the dissociation channel obtaining acetaldehyde and methyl radical. Rate constants for these reaction processes are plotted in Figure 10a. We can see that the formation of ethenol and propen-2-ol are more competitive than that of acetaldehyde and methyl radical. 1-Propenol is formed by H elimination from 1-hydroxypropyl radical. This process is competitive with the dissociation channel obtaining formaldehyde and ethyl radical. Rate constants for these reaction processes are plotted in Figure 10b. Obviously, the formation of 1-propenol is much more competitive through the whole temperature range investigated. Our model predicts a significant amount of ethenol and propenol produced at temperatures above 800 K.

Meanwhile, the rate constants fitted to a modified three-parameter Arrhenius expression are also provided. The rate constants in the temperature range of 200−3000 K at 760 Torr for the formations of ethenol (k_2), propen-2-ol (k_3), and 1-propenol (k_3'), in units of cm^3 molecule^{-1} s^{-1} are presented, respectively, as follows

$$k_2 = 1.88\times10^{-12}T^{0.05}\exp(-1723/T)$$

$$k_3 = 2.54\times10^{-14}T^{0.33}\exp(-1483/T)$$

$$k_3' = 4.84\times10^{-16}T^{1.05}\exp(-1888/T)$$

A strong curvature in the plot of the total rate constants is shown in Figure 9. Thus we fitted the predicted total rate constants with multiple reflection correction in two temperature ranges 200−800 K and 800−3000 K, respectively. The results in units of cm^3 molecule^{-1} s^{-1} are as follows

$$k_{200-800} = 6.07\times10^{-5}T^{-2.54}\exp(108/T)$$

$$k_{800-3000} = 7.11\times10^{-23}T^{3.38}\exp(-1097/T)$$

Channel switching is the cause of the strong curvature in the plot of the total rate constants between propene and OH. The dominant product branching ratios based on the theoretical rate constants computed at 760 Torr N_2 pressure are presented in Figure 11 as a function of temperature. The experimental values of these channels are not totally available. The branching ratios of the two products formaldehyde + ethyl radical and acetaldehyde + methyl radical are too small to compete throughout the entire temperature range investigated, so they are not included in the Figure 11. From Figure 10 we can also conclude that these two processes are not competitive.

In Figure 11, it is apparent that the complexes $CH_3CHOHCH_2$ and CH_2CHCH_2OH are the dominant products under about 700 K. The contribution of the two channels is almost 99% at 200 K. Although the contribution decreases with the temperature increasing, the value is still 64.4% at 700 K and the two branching ratios decrease rapidly from 500 to 1000 K. While from 500 to 800 K the branching ratios of ethenol, propen-2-ol, and 1-propenol increase steeply, and from 900 to 3000 K their ratios decrease slowly. The branching ratios of the three

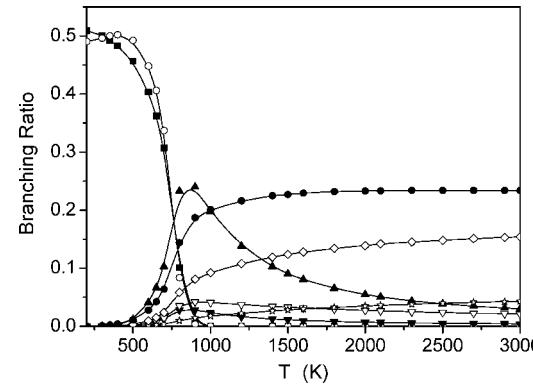

Figure 11. Product branching ratios at 1 atm of N_2 diluent. The lines with symbols represent the following: ■, $CH_3CHOHCH_2$; ○, CH_3CHCH_2OH; ▲, $CH_2CHOH + CH_3$; ▼, $CH_3COHCH_2 + H$; ▽, $CH_3CHCHOH + H$; ☆, $CH_3CH{=}CH + H_2O$; ◇, $CH_3C{=}CH_2 + H_2O$; ●, $CH_2CH{=}CH_2 + H_2O$.

products have not been obtained in experiments; Hoyermann and Sievert[18] measured the ratio of branching to the C_3H_6O (they assigned as acetone) channel to that of the C_2H_4O (they assigned as acetaldehyde) channel as 1:3.5 at room temperature. In our calculation the predicted maximum ratios of producing propenols (including propen-2-ol and 1-propenol) and ethenol are 0.071 and 0.24, respectively. The ratio is 1:3.38, which is acceptable in the experimental accuracy. From the tendency shown in Figure 11 we can explain the experimental values of Taatjes et al.[8] In the experiments, when the temperature is near 1000 K, the variational mole fraction of ethenol is not consistent with that of the ethene, that is because part of the ethenol is from the HO + propene reaction system. This can be obviously obtained from Figure 11. The branching ratio of ethenol is almost dominant from 700 to 1000 K, and this amount should be the extra part of the ethenol excluding that generated from the HO + ethene reaction system. This conclusion also confirms the fact that OH + ethene is not the sole source of ethenol, and the reaction of OH + propenol is another source of the observed propenol in this propene flame. So even if the mole fraction of ethene is small (at the burner distance from 0.0 to 1.0 mm in the experiment[8]), the amount of ethenol is significantly higher than expected. Flame calculations based on the present rate constants successfully account for the amount of ethenol and propenol observed by Taatjes et al.[8] Meanwhile, in the experiments, the amount of enols including ethenol and propenol from propene combustion flame decrease at a temperature above 1200 K. The reason is more likely that the channels of direct H-atom abstraction products turn out to be dominant at this temperature range. Over 1500 K, the reactions of H-atom abstraction processes have a contribution of almost 40%, in which the channel obtaining $CH_2CHCH_2 + H_2O$ is dominant, which is consistent with the experimental results.[10,14]

4. Conclusion

The potential energy profile and mechanism of the hydroxide radical reaction with C_3H_6 has been investigated at the PMP2/aug-cc-PVQZ//MP2/cc-PVTZ level of theory. The rate constants including the most important product branches starting from HO + C_3H_6 have been obtained in the temperature range of 200−3000 K using variational RRKM theory with the Variflex code. The available experimental kinetic data can be quantitatively reproduced by the calculation. The mechanisms of this reaction yielding enols established in this study considerably extend the results of previous theoretical investigations.

$CH_3CHOHCH_2$ and CH_2CHCH_2OH are the dominant products below 800 K. At high temperatures (above 800 K), a significant fraction of the total reaction leads to enols. Our calculated rate constant and branching ratio account successfully for the amount of enols observed in propene flame,[1] suggesting that ethenol and propenols should be included in the hydrocarbon combustion chemistry models. Our calculations confirm the importance of the hydrogen abstraction channels at temperatures above 900 K.

Acknowledgment. This work is supported by the National Natural Science Foundation of China (no. 20572073 and 20625331).

Supporting Information Available: Tables of total rate constants predicted at different temperatures and pressures and product branching ratios and a figure showing the predicted total rate constants with experimental results at 760 Torr. This information is available free of charge via the Internet at http://pubs.acs.org.

References and Notes

(1) Taatjes, C. A.; Hansen, N.; McIlroy, A.; Miller, J. A.; Senosiain, J. P.; Klippenstein, S. J.; Qi, F.; Sheng, L.; Zhang, Y.; Cool, T. A.; Wang, J.; Westmoreland, P. R.; Law, M. E.; Kasper, T.; Kohse-Höinghaus, K. *Science* **2005**, *308*, 1887.

(2) Cool, T. A.; Nakajima, K.; Mostefaoui, T. A.; Qi, F.; McIlroy, A.; Westmoreland, P. R.; Law, M. E.; Poisson, L.; Peterka, D. S.; Ahmed, M. *J. Chem. Phys.* **2003**, *119*, 8356.

(3) Erlenmeyer, E. *Chem. Ber.* **1880**, *13*, 305.

(4) Saito, S. *Chem. Phys. Lett.* **1976**, *42*, 399.

(5) Toullec, J.; El-Alaoui, M. *J. Org. Chem.* **1986**, *51*, 4054.

(6) Capon, B.; Guo, B. Z.; Kwok, F. C.; Siddhanta, A. K.; Zucco, C. *Acc. Chem. Res.* **1988**, *21*, 135.

(7) Hart, H. *Chem. Rev.* **1979**, *79*, 515.

(8) Taatjes, C. A.; Hansen, N.; Miller, J. A. *J. Phys. Chem. A* **2006**, *110*, 3254–3260.

(9) Atkinson, R.; Pitts, J. N. *J. Chem. Phys.* **1975**, *63*, 3591.

(10) Smith, G. P.; Fairchild, P. W.; Jeffries, J. B.; Crosley, D. R. *J. Phys. Chem.* **1985**, *89*, 1269–1278.

(11) Spangenberg, T.; Köhler, S.; Hansmann, B.; Wachsmuth, U.; Abel, B. *J. Phys. Chem. A* **2004**, *108*, 7527.

(12) Klein, Th.; Barnes, I.; Becker, K. H.; Fink, E. H.; Zabel, F. *J. Phys. Chem.* **1984**, *88*, 5052.

(13) Vakhtin, A. B.; Murphy, J. E.; Leone, S. R. *J. Phys. Chem. A* **2003**, *107*, 10055.

(14) Tully, F. P.; Goldsmith, J. E. M. *Chem. Phys. Lett.* **1985**, *116*, 345.

(15) Pastrana, A. V.; Carr, R. W. *J. Phys. Chem.* **1975**, *79*, 765.

(16) Senosiain, J. P.; Klippenstein, S. J.; Miller, J. A. *J. Phys. Chem. A* **2006**, *110*, 6960.

(17) Zellner, R.; Lorenz, K. *J. Phys. Chem.* **1984**, *88*, 984.

(18) Hoyermann, K.; Sievert, R. *Ber. Bunsen-Ges. Phys. Chem.* **1979**, *83*, 933.

(19) Diaz-Acosta, I.; Alvarez-Idaboy, J. R.; Vivier-Bunge, A. *Int. J. Chem. Kinet.* **1999**, *31*, 29.

(20) Alvarez-Idaboy, J. R.; Diaz-Acosta, I.; Vivier-Bunge, A. *J. Comput. Chem.* **1998**, *19*, 811.

(21) Szori, M.; Fittschen, C.; Csizmadia, I. G.; Viskolcz, B. *J. Chem. Theory Comput.* **2006**, *2*, 1575.

(22) Zhu, R. S.; Park, J.; Lin, M. C. *Chem. Phys. Lett.* **2005**, *408*, 25.

(23) Ruscic, B.; Wagner, A. F.; Harding, L. B.; Asher, R. L.; Feller, D.; Dixon, D. A.; Peterson, K. A.; Song, Y.; Qian, X.; Ng, C.-Y.; Lin, J.; Chen, W.; Schwenke, D. W. *J. Phys. Chem. A* **2002**, *106*, 2727.

(24) Afeefy, H. Y.; Liebman, J. F.; Stein, S. E. Neutral Thermochemical Data. In *NIST Chemistry WebBook, NIST Standard Reference Database Number 69*; Linstrom, P. J., Mallard, W. G. , Eds.; National Institute of Standards and Technology: Gaithersburg, MD, 2005; http://webbook.nist.gov.

(25) Holmes, J. L.; Lossing, F. P. *J. Am. Chem. Soc.* **1982**, *104*, 2648.

(26) Tureček, F.; Cramer, C. J. *J. Am. Chem. Soc.* **1995**, *117*, 12243.

(27) Tureček, F.; Havlas, Z. *J. Org. Chem.* **1986**, *51*, 4066.

(28) Hippler, H.; Viskolcz, B. *Phys. Chem. Chem. Phys.* **2000**, *2*, 3591.

(29) Sekušak, S.; Liedl, K. R.; Sabljić, A. *J. Phys. Chem. A* **1998**, *102*, 1583.

(30) Liu, G. X.; Ding, Y. H.; Li, Z. S.; Fu, Q.; Huang, X. R.; Sun, C. C.; Tang, A. C. *Phys. Chem. Chem. Phys.* **2002**, *4*, 1021.

(31) Piqueras, M. C.; Crespo, R.; Nebot-Gil, I.; Tomás, F. *J. Mol. Struct.* **2001**, *537*, 199.

(32) Villà, J.; González-Lafont, A.; Lluch, J. M.; Corchado, J. C.; Espinosa-García, J. *J. Chem. Phys.* **1997**, *107*, 7266.

(33) Sosa, C.; Schlegel, H. B. *J. Am. Chem. Soc.* **1987**, *109*, 7007.

(34) Sosa, C.; Schlegel, H. B. *J. Am. Chem. Soc.* **1987**, *109*, 4193.

(35) Alvarez-Idaboy, J. R.; Mora-Diez, N.; Vivier-Bunge, A. *J. Am. Chem. Soc.* **2000**, *122*, 3715.

(36) Galano, A.; Alvarez-Idaboy, J. R.; Ruiz-Santoyo, M. E.; Vivier-Bunge, A. *J. Phys. Chem. A* **2002**, *106*, 9520.

(37) Scoot, A. P.; Radom, L. *J. Phys. Chem.* **1996**, *100*, 16502.

(38) Huh, S. B.; Lee, J. S. *J. Chem. Phys.* **2003**, *118*, 3035.

(39) Frisch, M. J.; Trucks, G. W.; Schlegel, H. B. et al., *GAUSSIAN 03 B05*, Gaussian Inc.: Pittsburgh, 2003.

(40) (a) Wardlaw, D. M.; Marcus, R. A. *Chem. Phys. Lett.* **1984**, *110*, 230. J. Chem. Phys. 1985, *83*, 3462. (b) Klippenstein, S. J. *J. Chem. Phys.* **1992**, *96*, 367. (c) Klippenstein, S. J.; Marcus, R. A. *J. Chem. Phys.* **1987**, *87*, 3410.

(41) Gilbert, R. G.; Smith, S. C.; Jordan, M. J. T.UNIMOL program suite (calculation of fall-off curves for unimolecular and recombination reactions), Available from the authors: School of Chemistry, Sidney University, NSW 2006, Australia or by e-mail to gilbert_r@summer.chem.su.oz.au, 1993.

(42) Mokrushin, V.; Bedanov, V.; Tsang, W.; Zachariah, M. R.; Knyazev, V. D. *ChemRate version 1.16*; National Institute of Standards and Technology: Gaithersburg, MD, 20899..

(43) Klippenstein, S. J.; Wagner, A. F.; Dunbar, R. C.; Wardlaw, D. M.; Robertson, S. H. VARIFLEX: VERSION 1.00, 1999.

(44) (a) Klippenstein, S. J. *Chem. Phys. Lett.* **1990**, *170*, 71. (b) Klippenstein, S. J. *J. Chem. Phys.* **1991**, *94*, 6469. (c) Klippenstein, S. J. *J. Chem. Phys.* **1992**, *96*, 367.
(45) Robertson, S. H.; Wagner, A. F.; Wardlaw, D. M. *Faraday Discuss. Chem. Soc.* **1995**, *102*, 65.
(46) Cvetanovic, R. J. *J. Phys. Chem. Ref. Data* **1987**, *16*, 261.
(47) Ruscic, B.; Boggs, J. E.; Burcat, A.; Csaszar, A. G.; Demaison, J.; Janoschek, R.; Martin, J. M. L.; Morton, M. L.; Rossi, M. J.; Stanton, J. F.; Szalay, P. G.; Westmoreland, P. R.; Zabel, F.; Berces, T. *J. Phys. Chem. Ref. Data* **2005**, *34*, 573.
(48) Chase, M. W., Jr. *NIST-JANAF Thermochemical Tables*, 4th ed.; Woodbury, New York, 1998.
(49) Chase, M. W., Jr. *J. Phys. Chem. Ref. Data* **1998**, *9*, 1–1951.
(50) Furuyama, S.; Golden, D. M.; Benson, S. W. *J. Chem. Thermodyn.* **1969**, *1*, 363–375.
(51) Holmes, J. L.; Lossing, F. P. *J. Am. Chem. Soc.* **1982**, *104*, 2648–2649.
(52) Tsang, W. Heats of Formation of Organic Free Radicals by Kinetic Methods. In *Energetics of Organic Free Radicals*; Martinho Simoes, J. A., Greenberg, A., Liebman, J. F., Eds.; Blackie Academic and Professional: London, 1996; pp 22−58.
(53) Turecek, F. *J. Chem. Soc. Chem. Commun.* **1984**, *1374*, 1375.
(54) Atkinson, R. *Chem. Rev.* **1985**, *85*, 69.
(55) Wardlaw, D. M.; Marcus, R. A. *Chem. Phys. Lett.* **1984**, *110*, 230.
(56) Wardlaw, D. M.; Marcus, R. A. *J. Chem. Phys.* **1985**, *83*, 3462.
(57) Klippenstein, S. J. *J. Phys. Chem.* **1994**, *98*, 11459.
(58) Klippenstein, S. J. *Chem. Phys. Lett.* **1990**, *170*, 71.
(59) Klippenstein, S. J. *J. Phys. Chem.* **1994**, *98*, 1145.
(60) Holbrook, K. A.; Pilling, K. J.; Robertson, S. H. *Unimolecular Reactions*; Wiley: New York, 1996.
(61) Poling, B. E.; Prausnitz, J. M.; O'Connell, J. P. *The Properties of Gases and Liquids*, 5th ed.; McGraw-Hill: New York, 2001.
(62) Golden, D. M.; Smith, G. P.; McEwen, A. B.; Yu, C. L.; Eiteneer, B.; Frenklach, M.; Vaghjiani, G. L.; Ravishankara, A. R.; Tully, F. P. *J. Phys. Chem.* **1998**, *102*, 8598.
(63) Zhu, R. S.; Diau, E. G. W.; Lin, M. C.; Mebel, A. M. *J. Phys. Chem.* **2001**, *105*, 11249.
(64) Zhu, R. S.; Lin, M. C. *J. Chem. Phys.* **2003**, *118*, 4094.
(65) Zhu, R. S.; Lin, M. C. *ChemPhysChem.* **2004**, *5*, 1864–1870.
(66) Lee, C.; Yang, W.; Parr, R. G. *Phys. Rev.* **1998**, *B37*, 785.
(67) Eckart, C. *Phys. Rev.* **1930**, *35*, 1303.
(68) Miller, W. H. *J. Chem. Phys.* **1976**, *65*, 2216.
(69) Hirschfelder, J. O.; Wigner, E. *J. Chem. Phys.* **1939**, *7*, 616.
(70) Xu, S. C.; Zhu, R. S.; Lin, M. C. *Int. J. Chem. Kinet.* **2006**, *38*, 322.
(71) Tsang, W. *J. Phys. Chem. Ref. Data* **1991**, *20*, 221–273.

JP808574G